

Running title: miR166 controls *SPL/NZZ* in anther boundary

Corresponding author: Yuke He, Tel: 0086-2154924111, Fax: 0086-2154924015,
E-mail: ykhe@sibs.ac.cn

Title: microRNA166 monitors *SPOROXYTELESS/NOZZLE (SPL/NZZ)* for building of the anther internal boundary

1 **One sentence summary:** miR166 and its target *PHB* monitor *SPL/NZZ* gene
2 dynamically in construction of internal boundary and formation of dehiscence zones
3 in anthers.
4

5 The author(s) responsible for distribution of materials integral to the findings
6 presented in this article in accordance with the policy described in the Instructions for
7 Authors (www.plantphysiol.org) is: Yuke He (ykhe@sibs.ac.cn).

8

9 **Author contributions**

10 Y.H. designed studies and contributed to the original concept of the project; X.L. and
11 H. L. carried out experiments and result analysis; Q.Z. performed YFP expression
12 assay for protein-DNA interactions in tobacco leaves.

13

14

15 Xiaorong Li^{1,2,#}, Heng Lian^{1,#}, Qiuxia Zhao^{1,2} and Yuke He^{1,*}

16

17 ¹National Laboratory of Plant Molecular Genetics, Institute of Plant Physiology and
18 Ecology, Chinese Academy of Sciences, Shanghai 200032, China

19 ²University of Chinese Academy of Sciences, Beijing, China

20 # These authors contributed equally to this work.

21 * Author for correspondence (ykhe@sibs.ac.cn)

22

23 **Abstract**

24 The internal boundary between inner and outer microsporangia within anthers is
25 essential for male fertility of vascular plants. Dehiscence zones embedded in the
26 boundary release pollen for fertilization. However, the molecular mechanism
27 underlying boundary formation in anthers remains poorly understood. Here, we report
28 that microRNA166 (miR166) and its target *PHABULOSA* (*PHB*) regulate
29 *SPOROCTELESS/NOZZLE* (*SPL/NZZ*), which controls microsporogenesis. In
30 developing anthers of *Arabidopsis* (*Arabidopsis thaliana*), the expression domains of
31 miR165/6 and *SPL/NZZ* are overlapped and rearranged synchronously. Dominant
32 mutation of *PHB* suppresses *SPL/NZZ* expression in the adaxial sides of stamens,
33 resulting in a thickened boundary whereas activation of *MIR166g* upregulates
34 *SPL/NZZ* expression, leading to ectopic microsporogenesis in the boundary. *PHB*
35 limits the expression domains of *SPL/NZZ* to facilitate construction of the boundary
36 while miR166 preserves the expression domains of *SPL/NZZ* by inhibiting *PHB* to
37 allow the inner microsporangia to take shape. Subsequently, *PHB* activates key stem
38 cell maintainer *WUSCHEL* (*WUS*) in anthers to restrict the stomium cells to the
39 boundary so that dehiscence zones develop and release pollens properly. These
40 findings link adaxial/abaxial polarity to microsporogenesis in building of the internal
41 boundary of anthers, and thus advance the concepts underlying establishment of

1

42 internal structure of male organs.

43

44 **Key words:** anther structure; boundary; dehiscence zone; male fertility;
45 microsporangia; miR166, *PHB*, *SPL/NZZ*, stomium

46

47 **Introduction**

48 The stamen is an important reproductive lateral organ consisting of a four-lobed
49 anther that is anchored to the third whorl of a flower by a filament in many flowering
50 plants, including *Arabidopsis* (*Arabidopsis thaliana*) (Smyth et al., 1990; Goldberg et
51 al., 1993; Sanders et al., 1999; Scott et al., 2004). The four-lobed structure is mainly
52 composed of two inner microsporangia and two outer ones, also known as pollen sacs,
53 which are separated by a boundary where stomium regions and dehiscence zones
54 differentiate successively. Male fertility in many flowering plants relies on pollen
55 release from dehiscence zones in the boundary between inner and outer
56 microsporangia.

57 The formation of haploid cells (spores) in microsporangia by meiosis is called
58 sporogenesis (Yuan et al., 2015). Pollen grains are produced in the locules of
59 microsporangia (Ma, 2005; Feng and Dickinson, 2007; Feng and Dickinson, 2009).
60 Anther development in *A. thaliana* is divided into 14 stages (Sanders et al., 1999).
61 Stamen/anther primordia initiate from the floral apex at stage 1. Archesporial cells
62 then emerge in the four “corners” of the L2 layer at stage 2 and differentiate into
63 parietal and sporogenous cells in the four corners at stage 3. Concentrically organized
64 microsporangia are then generated in each corner of the anther at stage 5. At the same
65 time, the stomium region (also called the dehiscence zone) emerges between two
66 microsporangia in each half of the anther (theca) starting at stage 4. At stage 12, the
67 anther dehisces along the stomium regions and pollen grains are released for
68 pollination at anthesis.

69 The specification of the sporocytes represents a critical step during sporogenesis.
70 The *SPOROCTELESS/NOZZLE* (*SPL/NZZ*) gene, which encodes a nuclear protein,
71 was identified as a key regulator of this sporogenesis stage in *A. thaliana* (Schiefthaler

2

72 et al., 1999; Yang et al., 1999; Ito et al., 2004; Hord et al., 2006). The loss-of-function
73 mutant *spl* produces anthers lacking microsporangia. Two leucine-rich repeat
74 receptor-like protein kinases encoded by *BARELY ANY MERISTEMI* (*BAM1*)
75 and *BAM2* function in a regulatory loop with *SPL/NZZ* to restrict *SPL* expression to
76 the inner region of the locule (Zhao, 2009). Additionally, the *JAGGED* and *NUBBIN*
77 transcription factors function redundantly in adaxial cell proliferation and
78 differentiation in anthers (Dinney et al., 2006).

79 Along with germline determination, organ polarity establishment is a critical
80 issue that has recently been thoroughly investigated (Yang et al., 1999; Schiefthaler et
81 al., 1999). In some lateral organs, adaxial-abaxial polarity identity is precisely
82 regulated by two classes of antagonistic genes. The adaxial identity genes include the
83 HD-ZIP III family genes *REVOLUTA* (*REV*), *PHABULOSA* (*PHB*), *PHAVOLUTA*
84 (*PHV*), *CORONA* (*CNA*), and *ATHB8*, which are repressed by miR165/6 (Williams et
85 al., 2005; McConnell et al., 2001; Emery et al., 2003). In leaves and some other lateral
86 organs, HD-ZIP III genes are essential for the adaxial identity and function
87 antagonistically toward the abaxial identity genes, including the *KANADI* family
88 members, which positively regulate the expression of the *YABBY* group of abaxial
89 identity genes (Zhong, 1999; Eshed et al., 2001; Bowman, 2004; Wu et al., 2007; Liu
90 et al., 2011; Yang et al., 2014). The HD-ZIP III genes are also responsible for apical
91 identity during embryogenesis, and are antagonistic to *PLETHORA1/2* (*PLT1/2*)
92 (Smith and Long, 2010).

93 Although the effect of *PHB* and the other HD-ZIP III genes on leaf development
94 has been extensively studied, it remains poorly understood in anthers. In the stamen of
95 rice (*Oryza sativa*), the expression of *PHB3* (ortholog of *A. thaliana* *PHB*) is
96 rearranged during anther development (Zhong and Ye, 2004; Toriba et al., 2010).
97 *HYPONASTIC LEAF1* (*HYL1*) is an important player in miRNA processing (Wu et al.,
98 2007) and is required for establishment of stamen architecture with four
99 microsporangia in *Arabidopsis* (Lian et al., 2013).

100 Between inner and outer microsporangia is the boundary where stomium cells are
101 maintained to form dehiscence zones. *WUSCHEL* (*WUS*), originally identified as a

102 central regulator of stem cell maintenance, plays an important role in specification of
103 stomium cells (Deyhle et al., 2007). However, the molecular mechanism underlying
104 the formation of the boundary and dehiscence zone in anthers remains poorly
105 understood. Here, we report the dynamic expression programs of microRNA165/6
106 (miR165/6) and miR165/6-targeted *PHB* genes and their regulation to
107 *SPOROCTELESS/NOZZLE* (*SPL/NZZ*) gene during the formation of the boundary
108 and determination of stomium regions in anthers.

109

110

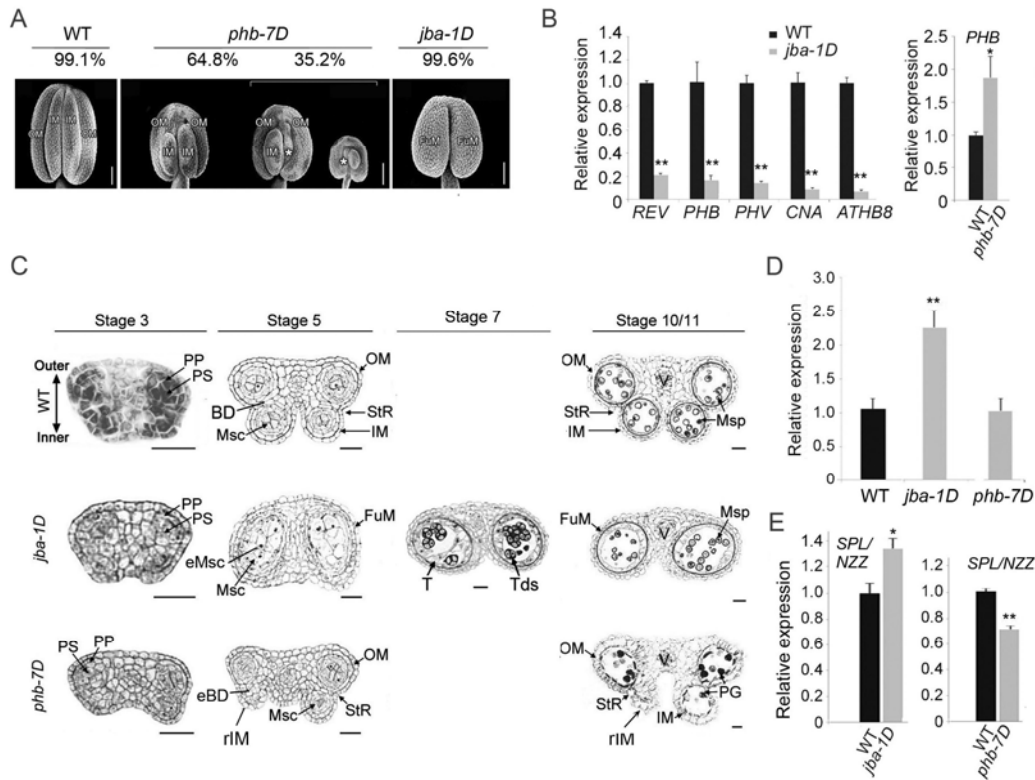
111 **Results**

112 ***MIR166g* activation causes ectopic microsporogenesis in the boundary between**
113 **inner and outer microsporangia**

114 To investigate whether and how miR165/6 regulate the formation of the boundary
115 between microsporangia, we chose the *jba-1D* mutant, in which the *MIR166g* gene
116 was activated (Williams et al., 2005). As expected, miR166 was upregulated and all
117 miR166-targeted HD-ZIP III genes were downregulated in the young inflorescences
118 (Supplemental Fig. S1A, B) and anthers (Fig. 1B) of the *jba-1D* mutant. In the
119 wild-type anthers, the four microsporangia were separated into two pairs (theca), each
120 of which contained an inner microsporangium and an outer microsporangium with a
121 boundary in between (Fig. 1A). Surprisingly, *jba-1D* anthers appeared to have only
122 two microsporangia instead of four. The boundary between inner and outer
123 microsporangia and dehiscence zones were not seen. However, the epidermal cells of
124 their connective tissues were not distinct from the wild type (Supplemental Fig. S1C).
125 Homozygous *jba-1D* plants were male-sterile.

126 We observed the internal structures of anthers and microsporangia using
127 transverse sections of early stamens (Fig. 1C). In the wild-type anther, the parietal and
128 sporogenous cells at stage 3 appeared in the two lateral regions, which were
129 bilaterally symmetrical while each was composed of one inner locule close to the
130 carpel and one outer locule close to the petal. The internal boundary between the inner
131 and outer locules were not observed at stage 2, but were seen at stage 3. The stomium
132 regions were located in the boundary furrow. The pollens were observed in the four
133 locules at stage 10/11. In *jba-1D* anthers, the two locules were much bigger than those
134 of the wild type (Fig. 1A, C; Table 1) and each of them contained more than twice the
135 number of microsporocytes that were in the wild-type locules (Fig. 1D), indicating
136 ectopic microsporogenesis in the enlarged microsporangia.

137 Close observation of the anthers at stage 7 showed that narrow creases still
138 developed down the center of some enlarged locules, which is where the two locules
139 would normally be separated and where anther dehiscence would occur. The presence
140 of the narrow creases marks the remnants of the boundary between inner and outer



141 microsporangia and indicates that the place of the boundary is occupied by
 142 microsporocytes. These results suggest that silencing of HD-ZIP III genes by
 143 *MIR166g* activation causes ectopic microsporocytes in the boundary.

144 We noticed that the boundary between inner and outer locules in the wild-type
 145 anthers formed after initiation of the parietal and sporogenous cells in the two lateral
 146 regions at stage 3 (Fig. 1C), meaning that inner and outer microsporangia are
 147 separated by the boundary after formation of the two lateral regions. The defects of
 148 boundary in *jba-1D* anthers appeared at stage 3 or earlier.

149

150 ***PHB* upregulation leads to the ectopic boundary tissues in inner microsporangia**

151 To test the effects of miR166-targeted genes on the boundary and microsporogenesis,
 152 we selected *phb-7D*, which is an miR166-resistant gain-of-function allele of *PHB*
 153 (Carlsbecker et al., 2010), as a representative mutant of the HD-ZIP III genes targeted
 154 by miR166. Compared with the wild-type microsporangia, the outer microsporangia
 155 in all *phb-7D* anthers were normal while the inner microsporangia were varied

156 between the anthers. Among the *phb-7D* anthers, 64.8% of anthers were categorized
157 as having a "mild" mutant phenotype because they had two small inner
158 microsporangia (Table 1; Fig. 1A), 30.2% of anthers were designated as having a
159 "medium" phenotype, since they lost one inner microsporangium, and about 5% of
160 anthers were regarded as having a "severe" phenotype, as they lost two inner
161 microsporangia.

162 To examine the internal structure of inner microsporangia, we observed the cross
163 sections of the *phb-7D* anthers with the "medium" phenotype. In these anthers, one
164 inner locule was aberrant (Fig. 1C), and the boundary between this inner locule and its
165 outer locule was thickened, thus showing small and/or empty inner locules. Numbers
166 of microsporocytes in these inner locules were much fewer than those of the wild type
167 (Fig. 1D). The anthers with mild and medium phenotypes were able to open and
168 released fewer pollen grains than the wild type; however, the anthers without inner
169 microsporangia failed to release pollens. These results suggest that upregulation of
170 *PHB* induce ectopic boundary tissues inside inner microsporangia, causing a
171 thickened boundary and aberrance or absence of inner microsporangia.

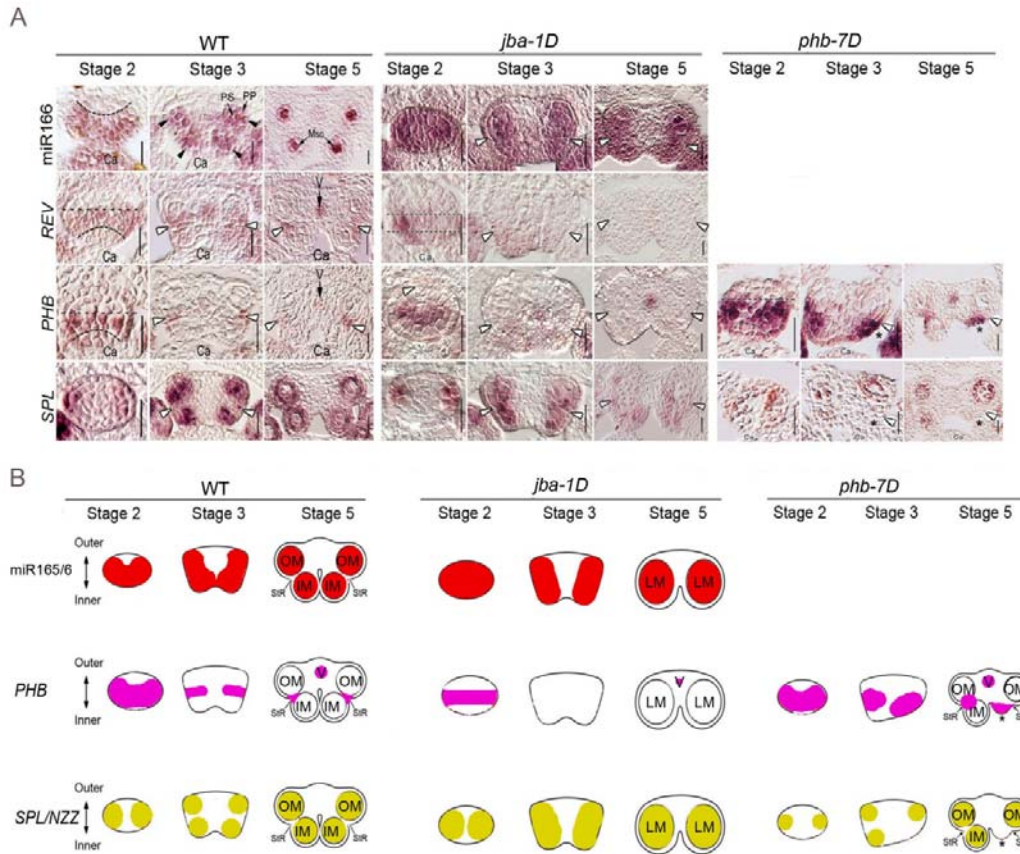
172

173 **Expression domains of miR165/6 and *SPL/NZZ* are overlapped in anthers**

174 *SPL/NZZ* is a key regulator of sporogenesis, especially regarding the specification of
175 microsporocytes derived from archesporial cells at stage 3 (Sanders et al., 1999). We
176 hypothesized that the expression of this gene was regulated by miR165/6. To test this
177 hypothesis, we compared expression levels of *SPL/NZZ* in the wild-type and *jba-1D*
178 anthers. The expression levels of *SPL/NZZ* in *jba-1D* anthers increased significantly
179 (Fig. 1E), coinciding with the downregulation of HD-ZIP III genes. These data
180 suggest that miR165/6 positively regulate the expression of *SPL/NZZ* in anthers.

181 To test whether miR166 regulates the expression domains of *SPL/NZZ* in anthers,
182 we conducted an RNA *in situ* hybridization experiment involving miR165/6 and
183 *SPL/NZZ*. In the wild-type anthers, miR165/6 accumulated in the lateral-adaxial
184 regions of stamens at stage 2 (Fig. 2A, B), forming two expression domains; and then
185 their expression domains appeared in the four corners of stamens at stage 3, and were

6



186 localized in the four microsporangia at stage 5. It thus appeared that the miR165/6
 187 domains were rearranged during anther development.

188 The expression domains of *SPL/NZZ* were largely overlapped with the miR165/6
 189 domains in the wild type. They were rearranged from the two lateral regions of
 190 anthers at stage 2, similar to miR165/6 domains, to the four corners at stage 3 and the
 191 microsporangia at stage 5. The difference is that *SPL/NZZ* expression domains in the
 192 two thecae appeared clearly in the regions surrounding microsporangia, in contrast
 193 with the miR165/6 domains that are strictly localized inside locules. This result
 194 suggests that that *SPL/NZZ* is involved in development of septum while miR165/6 is
 195 not.

196

197 **Expression domains of *PHB* and *SPL/NZZ* are opposite in anthers**

198 miR165/6 silence *PHB* in shoot and floral meristems. To investigate the regulation of
 199 the HD-ZIP III genes by *SPL/NZZ* in anthers, we compared expression levels of

200 *SPL/NZZ* in the wild-type and *phb-7D* anthers. The expression levels of *SPL/NZZ* in
201 *phb-7D* anthers declined significantly (Fig. 1E), coinciding with the upregulation of
202 HD-ZIP III genes. These data suggest that *PHB* and/or the other HD-ZIP III genes
203 negatively regulate the expression of *SPL/NZZ* in anthers.

204 In situ hybridization was adopted to show the expression patterns of *REV* and
205 *PHB* in developing anthers. In the wild-type anthers, *REV* and *PHB* were
206 preferentially expressed in the middle regions of the thecae as well as vascular tissue
207 in anthers at stage 2 (Fig. 2A, B); and then their expression domains appeared in the
208 boundary between inner and outer locules at stage 3, and were subsequently localized
209 in the stomium regions at stage 5. Therefore, the *REV* and *PHB* domains appear to
210 have rearranged during anther development.

211

212 **The mutation of *MIR166g* and *PHB* affects *SPL/NZZ* domains**

213 We wondered whether miR165/6 and the HD-ZIP III genes regulate the rearrangement
214 of *SPL/NZZ* domains. In *jba-1D* anthers, the miR165/6 domains were expanded and
215 occupied the whole locules at stage 2 (Fig. 2A, B). Then they formed the two domains
216 in the two thecae at stage 3, and subsequently became enlarged in the four locules at
217 stage 5 compared with the wild type. By contrast, the expression domains of *PHB* and
218 *REV* were smaller in the lateral regions at stage 2 compared with those of the wild
219 type, and disappeared in anthers at stages 3 and 5. The miR165/6 domains of *jba-1D*
220 anthers at stage 3 are consistent with their enlarged microsporangia. Interestingly,
221 *SPL/NZZ* domains at stage 3 were seen in two lateral regions of early stamens, and
222 dispersed in the two locules at stage 5. *SPL/NZZ* domains were matched with the
223 enlarged microsporangia. This observation suggests that miR166 maintains *SPL/NZZ*
224 domains and facilitates microsporogenesis in inner microsporangia.

225 In *phb-7D* anthers, *PHB* domains were expanded and occupied most of the thecae
226 in the adaxial regions of anthers at stage 2 (Fig. 2A, B). Then they formed the two
227 clear domains in the boundary at stage 3, and subsequently became enlarged in the
228 stomium regions at stage 5 compared with the wild type. Interestingly, the enlarged
229 *PHB* domains of *phb-7D* anthers at stage 3 are matched with their thickened boundary.

8

230 Correspondingly, *SPL/NZZ* domains were smaller in stamen primordia at stages 2, 3,
231 and 5 compared with the wild type. Together, these results suggest that PHB limits
232 *SPL/NZZ* domains and promotes the formation of stomium in the boundary.

233

234 ***SPL/NZZ* acts downstream of miR166 and the HD-ZIP III genes**

235 To verify the genetic interaction between HD-ZIP III genes and *SPL/NZZ*, we crossed
236 the *spl* mutant with the *phb-7D* and *jba-1D* mutants. The *spl* seedlings and flowers
237 looked similar to the wild type (Supplemental Fig. S2A, B) but their anthers did not
238 form microsporocytes as previously described (Yang *et al.*, 1999) with the similar
239 cells on the adaxial and abaxial surfaces (Supplemental Fig. S2C-E). At anthesis, the
240 *spl* anthers consisted of highly vacuolated parenchyma cells, without any
241 microsporangia or pollen (Fig. 3A–E). The anthers of the *spl phb-7D* double mutants
242 resembled those of the *spl* mutant (i.e., microsporangia and locules were absent).
243 Similar to the *spl* anthers, the *spl jba-1D* anthers completely lacked microsporangia.
244 These results suggest that *SPL/NZZ* acts downstream of the HD-ZIP III genes.

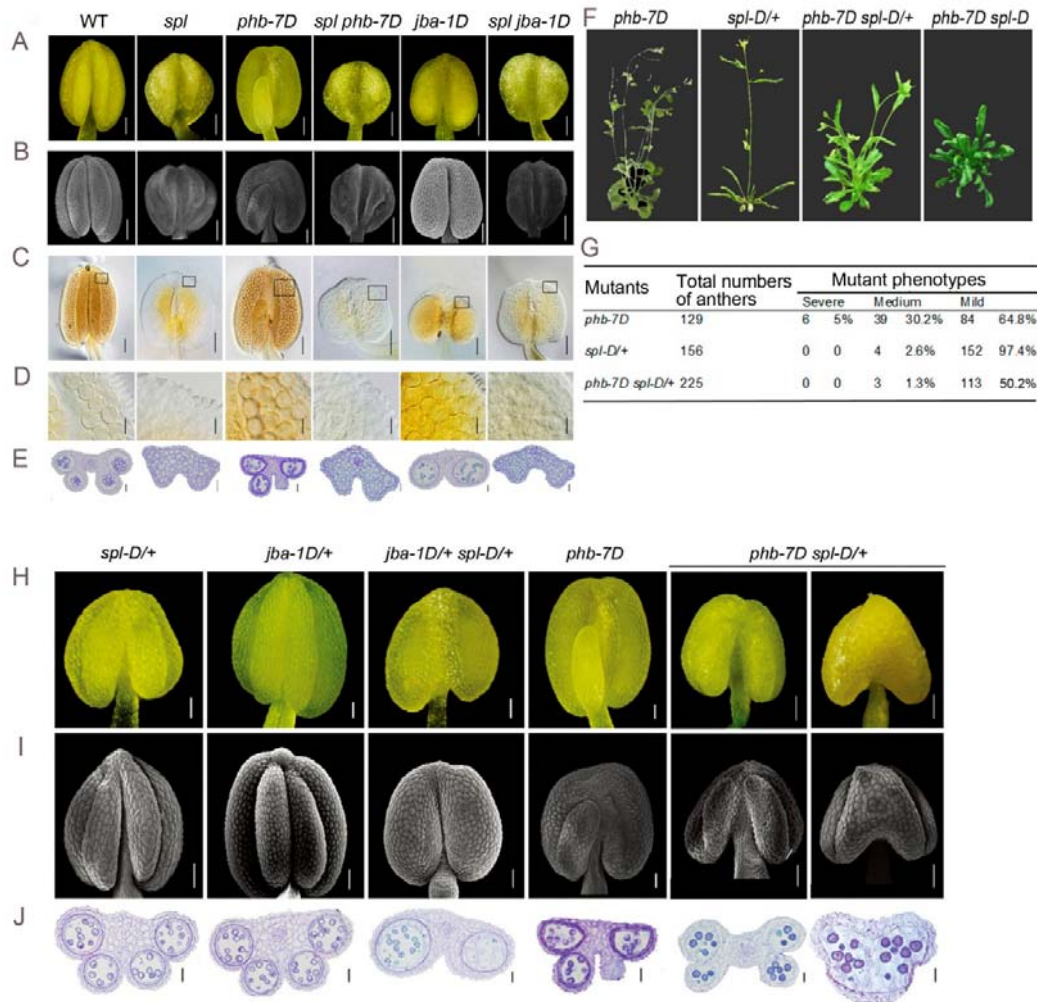
245

246 **PHB binds the promoter of *SPL/NZZ***

247 The HD-ZIP III genes regulate the downstream genes by directly binding to the
248 conserved motifs in the promoters of auxin biosynthesis gene (Brandt.*et al.*, 2012).
249 Within the upstream and 5' untranslated regions of *SPL/NZZ*, there are six putative
250 binding sites (Fig. 4A). To test the binding affinity between PHB and these motifs, we
251 purified MBP-PHB fusion proteins (Supplemental Fig. S3A). The EMSA data shows
252 that PHB was bound to the motif (Supplemental Fig. S3B, C). Moreover, the binding
253 signal between PHB and the motif is enhanced with increased concentrations of probe
254 (Supplemental Fig. S3D). Then, we used this reaction system to verify the binding
255 possibility between PHB and the *SPL/NZZ* promoter. S4, S5, and S6 sites showed
256 binding affinity (Fig. 4B). Among them, site S4 exhibited specific binding affinity
257 with PHB under the competitive condition with non-labeled probes and mutated
258 probes (Fig. 4C, D).

259 To confirm the direct interaction between PHB and *SPL/NZZ* loci *in vivo*, we

9

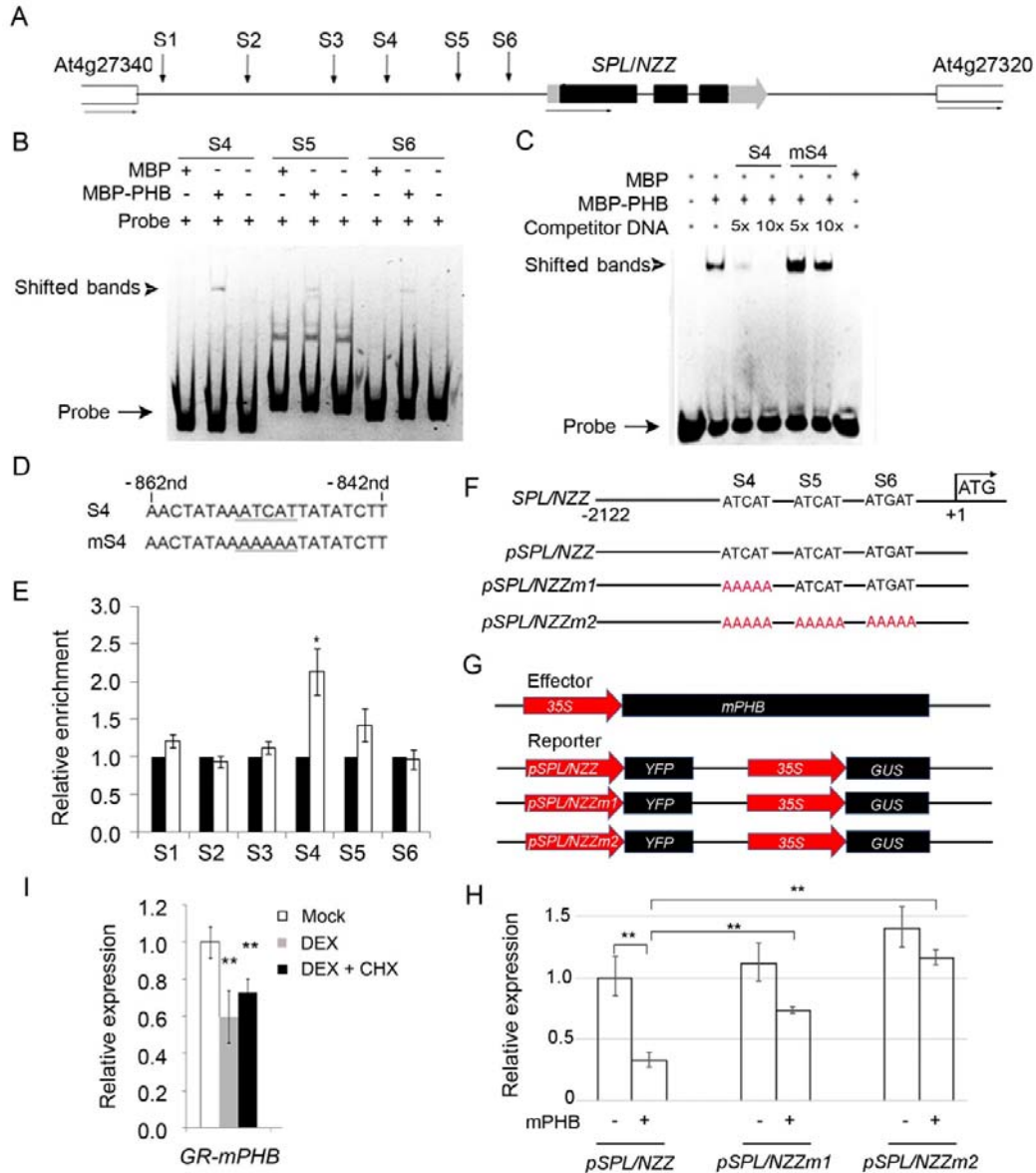


260 conducted a ChIP assay using a transgenic line expressing the 3×Flag-mPHB fusion
 261 constructs under the control of the 35S promoter. The chromatin extracted from the
 262 inflorescences was immunoprecipitated with anti-Flag antibodies, and the abundance
 263 of approximately 150-bp regions containing PHB binding sequences was measured by
 264 quantitative PCR (qPCR). The site S4 in the *SPL/NZZ* promoter was enriched near
 265 two-fold in the plants with 3×Flag-mPHB after being immunoprecipitated by the
 266 corresponding antibody (Fig. 4E). However, the other sites were not enriched
 267 significantly. These data suggest that PHB directly binds the *SPL/NZZ* promoter *in*
 268 *vivo*.

269

270 ***SPL/NZZ* expression is suppressed by *PHB* upregulation**

271 To verify the function of PHB in its regulation to *SPL/NZZ*, a reporter transaction
 10



272 assay in *Nicotiana benthamiana* leaves was performed. The vectors that harbor
 273 *pSPL/NZZ* (the promoter of *SPL/NZZ*) *pSPL/NZZm1* (*pSPL/NZZ* with mutated
 274 binding site S4), and *pSPL/NZZm2* (*pSPL/NZZ* with mutated binding sites S4, S5, S6)
 275 were designed to drive YFP reporters (Fig. 4F, G). In the presence or absence of PHB,
 276 YFP were transiently expressed in tobacco plants with *pSPL/NZZ*, *pSPL/NZZm1*, and
 277 *pSPL/NZZm2*. The YFP expression levels declined in *pSPL/NZZ* plants when
 278 co-expressed with PHB; and YFP expression levels were much higher in
 279 *pSPL/NZZm1* and *pSPL/NZZm2* plants compared with those of *pSPL/NZZ* plants (Fig.

280 4H). This result revealed that PHB negatively regulated *SPL/NZZ* by directly binding
281 to the *SPL/NZZ* promoter.

282 Next, we explored the possibility that PHB represses *SPL/NZZ* expression in
283 *Arabidopsis* using an inducible expression system based on the posttranscriptional
284 activation of the rat GR. A *GR-mPHB* construct was transformed into *Arabidopsis*
285 plants. In the inflorescences of the transgenic plants expressing *GR-mPHB*, *SPL/NZZ*
286 expression levels declined significantly following a 6-h treatment with dexamethasone
287 and a 6-h treatment with DEX and CHX (Fig. 4I). We conclude that *SPL/NZZ*
288 transcription is repressed following *PHB* induction.

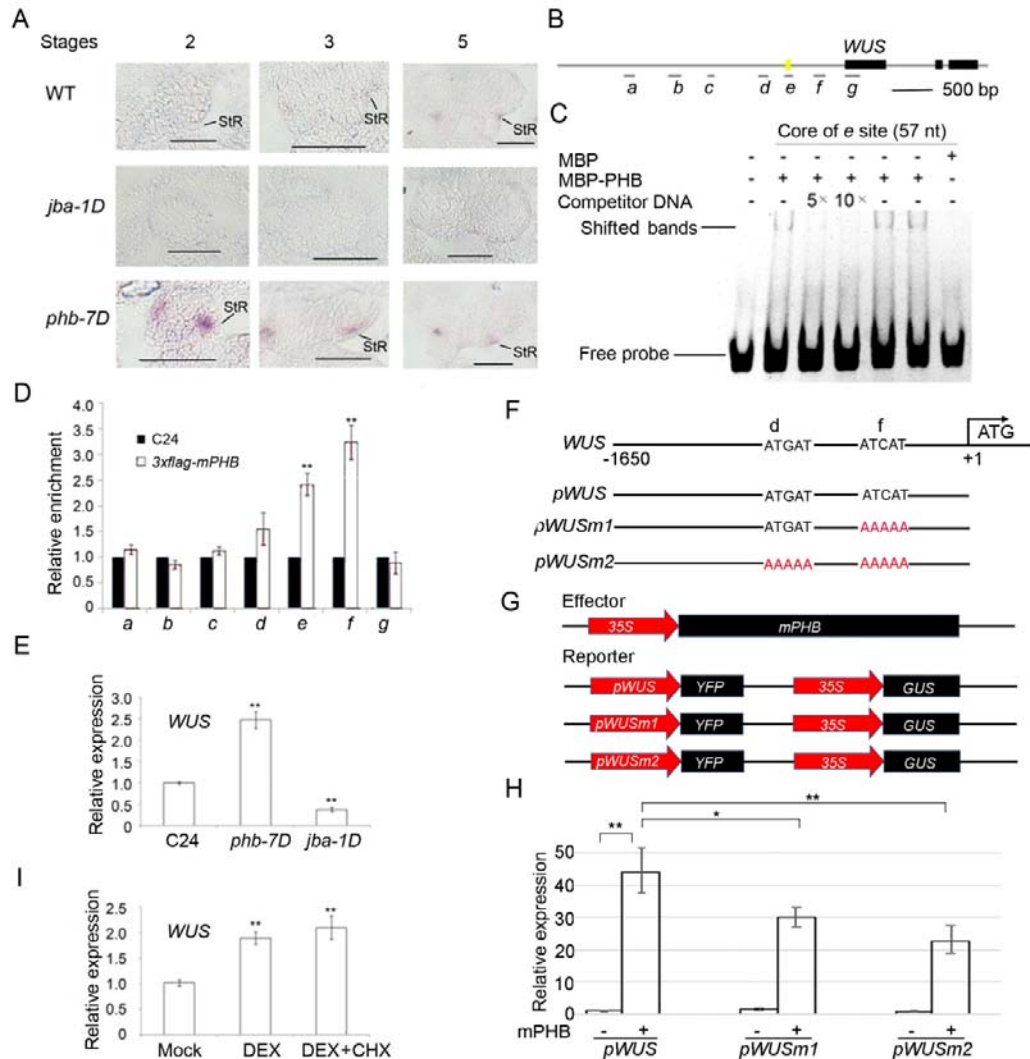
289

290 **PHB activates *WUS* to maintain stomium cells**

291 The key regulator of stem cell homeostasis *WUSCHEL* (*WUS*) is the only known
292 regulator that engages in the initiation and development of stomium cell in
293 *Arabidopsis* (Bäurle and Laux, 2005). To examine how *MIR166g* activation affects the
294 formation of the stomium region in the boundary, we performed in situ hybridization
295 of *WUS* using the anthers at different stages. In the wild-type anthers, the *WUS* signal
296 was faint in the boundary furrow between inner and outer locules at stage 3 (Fig. 5A),
297 and became stronger and expanded at stage 5. This experiment reveals that the
298 stomium is in the boundary furrow between inner and outer microsporangia. In
299 *jba-1D* anthers, *WUS* signal was not detected at stages 2, 3, and 5. In *phb-7D* anthers,
300 by contrast, *WUS* domains were expanded beyond the internal boundary at stage 2,
301 but became weaker and smaller at stages 3 and 5. This result implies that PHB
302 restricts stomium to the boundary between inner and outer microsporangia.

303 To determine whether PHB directly binds to the *WUS* promoter, we performed
304 EMSA experiments. There are seven putative binding sites for PHB within the
305 promoter region of *WUS* (Fig. 5B). A 57-bp regulatory region (-655bp ~ -712bp)
306 confers *WUS* transcription in the SAM (Shoot Apical Meristem) stem cell niche
307 (Bäurle et al., 2005). As expected, PHB shows binding affinity with this regulatory
308 region (Fig. 5C). Then, a ChIP experiment showed that two DNA fragments are
309 enriched 2-4 times in the transgenic lines with $3\times$ Flag-*mPHB* (Fig. 5D). These results

12



310 confirm that PHB binds the promoter of *WUS*.

311 RT-qPCR shows that *WUS* was upregulated in *phb-7D* anthers but
 312 down-regulated in *jba-1D* anthers (Fig. 5E). We wondered whether induction of *PHB*
 313 expression affects *WUS* expression level.

314 The transient transcription assay was applied to verify the regulation of PHB to
 315 *WUS*. The *YFP* gene was driven by *pWUS* (the wild-type *WUS* promoter), *pWUSm1*
 316 (mutant *WUS* promoter with mutant binding site f), and *pWUSm2* (mutant binding
 317 sites d and f) (Fig. 5F, G). *YFP* expression was upregulated in *pWUS* plants upon
 318 co-transformation with *p35S::mPHB* (Fig. 5H); and was reduced in *pWUSm1* and
 319 *pWUSm2* plants when PHB was co-expressed with *WUS*. This result indicated that

320 PHB positively regulated *WUS* (Fig. 5H).

321 We next used an inducible expression system based on posttranscriptional
322 activation of the rat GR (Glucocorticoid Receptor). A *GR-mPHB* construct was
323 transformed into Arabidopsis plants. In the inflorescences of the transgenic plants
324 expressing *GR-mPHB*, the expression levels of *WUS* were significantly increased
325 following a 6-h treatment with dexamethasone and a 6-h treatment with DEX and
326 CHX (Fig. 5I). We conclude that *PHB* acts upstream of *WUS* to maintain stomium
327 stem cells.

328

329 ***spl-D* aggravates the phenotype of *jba-1D/+* plants**

330 *spl-D* is a dominant mutant of the *SPL/NZZ* gene. Homozygous *spl-D* plants produced
331 upwardly curved leaves (Supplemental Fig. S4A) and never bolted as noted in earlier
332 studies (Li *et al.*, 2008). Therefore, we used the anthers of heterozygous *spl-D* plants
333 (*spl-D/+*) (Supplemental Fig. S4B) for the following study. The *spl-D/+* plants
334 flowered (Fig. 3F), and set seeds because they had normal anthers with four
335 microsporangia (Fig. 3H). To further define the relationship between the HD-ZIP III
336 genes and *SPL/NZZ*, we crossed *jba-1D/+* with *spl-D/+* plants. Homozygous *jba-1D*
337 anthers were male sterile and could not be used for genetic analysis while the
338 heterozygotic *jba-1D/+* anthers resembled the wild-type anthers with four
339 microsporangia. The heterozygotic *jba-1D/+ spl-D/+* plants were individually
340 identified by PCR and self-pollinated to generate F₂ segregating populations, some of
341 which were selected for genetic analysis. The *jba-1D/+ spl-D/+* plants formed anthers
342 with only two enlarged microsporangia (Fig. 3H, I). These anthers had ectopic
343 microsporangia in the place of an internal boundary (Fig. 3J), just like the
344 homozygous *jba-1D* anthers. Meanwhile, the expression levels of *SPL/NZZ* in
345 *jba-1D/+ spl-D/+* anthers increased substantially compared with those of *jba-1D/+*
346 anthers (Supplemental Fig. S5). Our observations provide molecular support that
347 *spl-D/+* aggravates the mutant phenotype of *jba-1D/+* in terms of boundary defects.

348

349 ***spl-D* partially rescues the mutant phenotype of *phb-7D***

14

350 To verify the epistatic effect of *SPL/NZZ* on *PHB*, we used the *phb-7D* mutant as the
351 female parent to cross with the *spl-D/+* mutant. The *phb-7D/+ spl-D/+* plants in the
352 F₁ population were selected using *phb-7D* dCAPS (derived cleaved amplified
353 polymorphic sequences) primers and *spl-D* genotyping primers. Similarly, the F₁
354 plants were self-fertilized to obtain F₂ segregating populations, which included
355 *phb-7D*, *spl-D/+*, *phb-7D spl-D/+*, and *phb-7D spl-D* plants. Like the *spl-D* mutant,
356 *phb-7D spl-D* plants did not flower. Hence, we were unable to analyze the *phb-7D*
357 *spl-D* anthers. The *phb-7D spl-D/+* plants flowered (Fig. 3F) like the *phb-7D* mutant
358 but their flowers lacked petals. These plants produced upwardly-curved leaves like the
359 *spl-D* mutant plants. Surprisingly, the anthers without inner microsporangia in *phb-7D*
360 *spl-D/+* plants disappeared while almost all inner microsporangia contained
361 microsporocytes (Fig. 3G). 50% of the anthers of the *phb-7D spl-D/+* plants showed
362 the thinner boundary than *phb-7D* anthers (Fig. 3H-J), with inner microsporangia
363 smaller than those of the wild-type anthers but larger than those of the *phb-7D* anthers.
364 Meanwhile, the expression levels of *SPL/NZZ* in *phb-7D spl-D/+* anthers increased
365 substantially compared with those of *phb-7D* anthers (Supplemental Fig. S5). The
366 changes in *phb-7D spl-D/+* plants suggest that the mutant phenotypes of *phb-7D* allele
367 were partially recovered in the thickened boundary and aberrant inner microsporangia.
368 The remaining anthers contained two enlarged inner microsporangia that were
369 partially joined. A subsequent analysis of a semi-thin section revealed that the joined
370 inner microsporangia were separated by a septum. Interestingly, the anthers with
371 joined inner microsporangia opened and released pollen grains even though their
372 seedset rate was much lower than that of the wild-type anthers. These results suggest
373 that the mutant phenotypes of *phb-7D* plants are partially rescued by *spl-D/+*.

374

375

376 **Discussion**

377

378 **miR165/6 monitors *SPL/NZZ* for boundary building**

379 HD-ZIP III genes such as *PHB* and *REV* are essential for the adaxial identity of lateral
380 organs. In *Arabidopsis*, expression domains of *PHB* and *REV* are found to be
381 rearranged during stamen development. The inference is that the rearrangement of
382 expression domain of HD-ZIP III genes during anther development is a general event
383 in vascular plants. Importantly, this type of rearrangement of expression domains is
384 controlled by miR165/6 through post-transcriptional gene silencing. Originally,
385 miR165/6 accumulates in the adaxial regions of stamen primordia (stage 2), is
386 redistributed in the lateral sides of early stamen (stage 3), and then rearranged to the
387 microsporangia in the late stamen (stage 5). Meanwhile, *PHB* and *REV* expression
388 domains were moved to the boundary regions between inner and outer microsporangia
389 in the early stamen, and located in stomium regions within the late stamen. Therefore,
390 temporal and spatial expression patterns of *PHB* and *REV* expression domains show
391 an opposite trend to that of miR165/6 accumulation.

392 *SPL/NZZ* expression domains overlapped with the domain of miR165/6
393 accumulation. Both domains are rearranged in different directions from the *PHB*
394 domains. miR165/6 and *SPL/NZZ* domains are moved from the lateral regions of
395 stamen primordia to stamen corners and then to microsporangia, while *PHB* domain
396 migrated from the middle regions of stamen primordia to the boundary between inner
397 and outer microsporangia and then to stomium regions. *MIR166g* activation causes
398 the misplacement of *SPL/NZZ*, leading to the ectopic formation of microsporocytes in
399 the place of boundary. Importantly, the absence of the boundary undoes the formation
400 of stomium and dehiscence zones, resulting in male sterility. The formation of the
401 boundary is therefore a prerequisite for differentiation of the stomium region.

402 Regulation of miR65/6 to *SPL/NZZ* is accomplished by HD-ZIP III genes. *PHB*
403 inhibits *SPL/NZZ* in inner microsporangia by binding to the promoter to build the
404 boundary. The dominant mutation of *PHB* causes shrunken domains of *SPL/NZZ* in
405 the whole or part of the inner microsporangia and disrupts two important

16

406 developmental events: thickening of the boundary between inner and outer
407 microsporangia and microsporogenesis in inner microsporangia. By inhibiting SPL
408 activity, PHB blocks cell formation of microsporocytes in the boundary, and
409 facilitates its formation. The *spl-D* allele aggravates the *jba-1D* mutant phenotype in
410 terms of boundary defects, but partially rescues the *phb-7D* phenotype in terms of
411 boundary thickening. Considering that miR165/6 and PHB act upstream of *SPL/NZZ*,
412 we conclude that miR165/6 monitors *SPL/NZZ* domains for building of the boundary.

413 Archesporial cells emerge in the four corners of early stamen (Feng and
414 Dickinson, 2007; 2009). We observed the parietal and sporogenous cells in the two
415 lateral regions of early stamens at stage 2 before the stamen primordia are separated
416 into the four corners. The occupation of miR165/6 and *SPL/NZZ* domains in the
417 lateral regions of early stamens implies that there is meristem-like tissue in the
418 boundary from where an archesporial cell is initiated and divides, timely forming two
419 lateral regions of early stamens. This meristem-like tissue could be the stomium
420 region. The stomium would thus assume some aspect of apical meristem function
421 (Deyhle et al., 2007). It is interesting to uncover a molecular connection between
422 embryonic meristem and the stomium region.

423

424 **PHB determines the formation of stomium in anthers**

425 In rice, the expression of *PHB3* (rice homolog of *PHB*) marks the stomium region as
426 an adaxial one (Toriba et al., 2010). We asked whether *PHB* of Arabidopsis determines
427 the formation of stomium. Notably, *PHB* domains in stomium regions of Arabidopsis
428 anthers at stages 3 and 5 are the same as *PHB3* domains. The inference is that
429 monocots and dicots share similar adaxial regions in the boundary. *WUS* expression
430 indicated that stomium cells are localized in the boundary furrow between inner and
431 outer microsporangia. *WUS* expression is not expressed in anther primordium a stage
432 1, but appears at stage 2 and continues until stage 11 when the stomium cells start to
433 display specific differentiation (Deyhle et al., 2007). We detected *WUS* expression in
434 boundary furrows at stage 2. This suggests that stomium regions are initiated at stage
435 3 or before.

17

436 In the *jba-1D* mutant, the *SPL/NZZ* domain is expanded to the place of the
437 boundary containing the stomium regions, concurrent with the appearance of ectopic
438 microsporocytes and absence of the dehiscence zones. In the *phb-7D* mutant,
439 *SPL/NZZ* expression domains were shrunk, concurrent with the thickening of the
440 boundary and the presence of dehiscence zones. Given that PHB acts upstream of
441 *WUS*, we propose that PHB determines the formation of stomium through *WUS*.

442 Our genetic evidence indicates that PHB is required for boundary building. In
443 Arabidopsis, adaxial thecae and abaxial connectives differentiate from the stamen
444 primordia. During theca development, the boundary between inner and outer
445 microsporangia is the adaxial region as marked by *PHB* domains; stomium embedded
446 in the boundary is the adaxial region as indicated by *PHB*. *PHB* domains in anthers
447 become centralized progressively from stage 2 to 5. We suggest that *PHB* restricts the
448 stomium to the boundary, so that the inner microsporangia take shape for
449 differentiation of microsporocyte cells.

450

451 **Crosstalk between miR165/6 pathway and *SPL/NZZ* links polarity to**
452 **microsporogenesis**

453 The internal structure of an anther with four microsporangia largely relies on the
454 balance between the HD-ZIP III genes and *SPL/NZZ*. As such, there is considerable
455 crosstalk between genes that control adaxial identity and microsporogenesis. In the
456 stamen primordia (stage 2), miR165/6 accumulates in the lateral regions while
457 *SPL/NZZ* is preferentially expressed in the lateral regions. Then, miR165/6
458 accumulation and *SPL/NZZ* domains are rearranged simultaneously to the corners of
459 stamen primordia at stage 3 and to the microsporangia at stage 5. Meanwhile, the
460 expression domains of miR165/6-targeted *PHB* are redistributed to the boundary
461 between inner and outer microsporangia at stage 3 and to stomium at stage 5. During
462 the translocation of the adaxial regions in anthers, miR165/6 acts to control the
463 expression domains and activity of *SPL/NZZ* by silencing HD-ZIP III genes and
464 maintaining the balance between PHB and *SPL/NZZ* for programming of the two
465 developmental events: microsporogenesis in microsporangia and formation of the

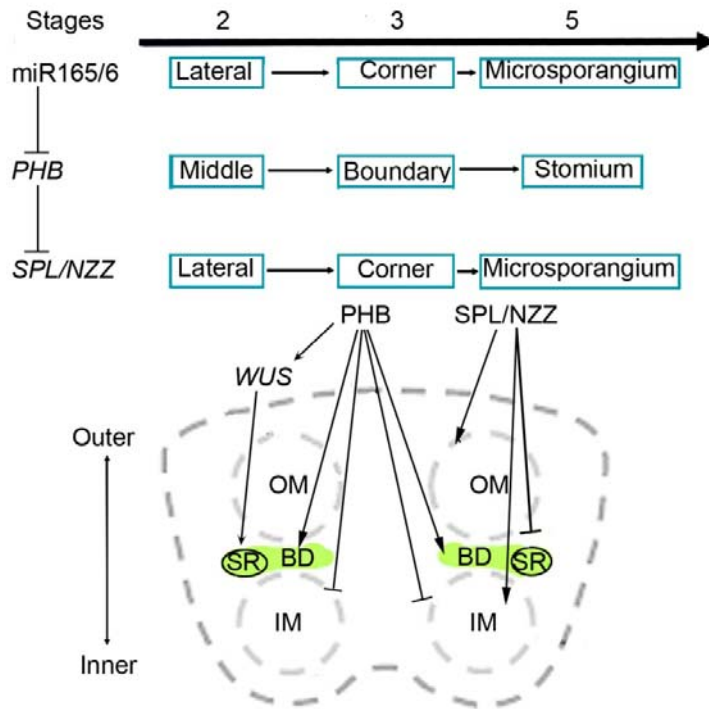
18

466 boundary between inner and outer microsporangia. During this process, PHB
467 determines boundary formation by inhibiting the *SPL/NZZ* gene. Thus, the crosstalk
468 between the genes that control adaxial polarity and microsporogenesis constitutes an
469 important link between adaxial polarity in the internal boundary of anthers and
470 microsporogenesis in microsporangia.

471 Arabidopsis and rice are different in anther shape and size, but they program
472 similar developmental events. To illustrate the regulatory roles of miR165/6 and
473 *SPL/NZZ* in establishment of internal structure in anthers, we refine the early stages
474 of anther development as follows. Initially, two adaxial regions are established in the
475 place adjacent to the floral meristem (at stage 1 and earlier), and develop into the two
476 thecae while abaxial regions form in the place opposite to it and develop into the
477 connectives (Feng and Dickinson, 2007; Feng and Dickinson, 2009; Toriba et al.,
478 2010) Then, the newly-formed adaxial regions are formed in the middle regions of
479 two thecae and subsequently turn into the boundary between inner and outer
480 microsporangia. In the boundary furrows, stomium regions are maintained and
481 become another newly-formed adaxial region. According to these developmental
482 events, we propose a model for the regulation of miR165/6 to *SPL/NZZ* in the
483 formation of the boundary between microsporangia in anthers (Fig. 6). In general,
484 there are three dimensions of anther formation: miR165/6 modulates *SPL/NZZ* by
485 *PHB*; miR165/6, *PHB*, and *SPL/NZZ* domains are rearranged in the developing
486 anthers; and PHB controls the building of the internal boundary by inhibiting
487 *SPL/NZZ* and determines the formation of stomium by activating *WUS*. Therefore,
488 miR165/6 balances the expression of *PHB* and *SPL/NZZ* to link adaxial polarity to
489 microsporogenesis in anthers

490

491



492 **Methods**

493

494 **Plant materials and growth conditions**

495 *Arabidopsis* (*Arabidopsis thaliana*) mutants used in this study included *jba-1D*,
 496 *phb-7D*, *spl*, and *spl-D* (Supplemental Table S1). The seeds of wild type and mutants
 497 were surface-sterilized in 70% (v/v) ethanol for 1 minute and then in 1% (v/v) NaOCl
 498 for 10 min, after that they were washed four times in sterile distilled water. Seeds
 499 were then placed on the surface of 1% (w/v) agar-solidified Murashige and Skoog
 500 medium. Plates were sealed with Parafilm, incubated at 4°C in darkness for 3 to 4
 501 days, and then moved to a growth chamber at 22°C with a 16-h photoperiod. The *spl*
 502 *jba-1D*, *spl phb-7D*, *jba-1D/+ spl-D/+*, *phb-7D spl-D/+*, and *phb-7D jba-1D* double
 503 mutants were generated by crossing the corresponding mutants and then characterized
 504 by culturing in a medium supplemented with the appropriate antibiotic as well as by
 505 PCR and phenotypic analyses.

506

507 **Scanning electron microscopy**

508 Flowers and inflorescences were fixed in FAA [50% (v/v) ethanol, 5% (v/v) acetic
509 acid, and 3.7% (v/v) formaldehyde] and dried. They were then dissected under a
510 stereo microscope and mounted on sample stubs for scanning electron microscopy
511 (SEM). Mounted anthers were coated with palladium-gold and then examined using a
512 JSM-6360LV scanning electron microscope (JEOL, Tokyo, Japan) with an
513 acceleration voltage of 7-15 kV.

514

515 **Histology and light microscopy**

516 Flowers (inflorescences) of 5- to 6-week-old wild-type and mutant plants were fixed
517 in FAA and embedded in paraffin (Sigma, St. Louis, MO, USA), after which 7- μ m
518 sections were stained with 0.05% (w/v) toluidine blue (Sigma) at 37°C for 15 min.
519 The stained sections were washed in water and treated with Histo-Clear (National
520 Diagnostics, Atlanta, GA, USA), which is a non-toxic histological clearing agent to
521 remove paraffin. To analyze semi-thin sections, samples fixed in FAA were embedded
522 in epoxy resin. Glass knives were used to prepare 2- μ m sections, which were then
523 affixed to glass slides and stained with 0.05% (w/v) toluidine blue.

524 Samples and sections were observed using a BX 51 wide-field microscope
525 equipped with UPlanSAPO series objectives and a cooled DP71 camera (Olympus,
526 Tokyo, Japan) and with a Stemi 2000 stereo microscope (Zeiss, Oberkochen,
527 Germany). To observe the hybridization signal after *in situ* hybridization, slides were
528 mounted in water and analyzed by differential interference contrast (DIC) microscopy.
529 For anther imaging, Image-Pro Express version 5.1 software (Media Cybernetics,
530 Bethesda, MD, USA) was used to extend the depth of field.

531 For whole-mount clearing analysis, anthers were collected under a stereo
532 microscope and immersed in clearing solution (2 g phenol, 2 g chloral hydrate, 2 ml
533 75% lactic acid, 2 g oil of clove, and 1 ml xylene) for several minutes. The specimens
534 were analyzed by DIC microscopy.

535

536 ***In situ* hybridization**

537 Flower sections (7 μ m thick) from wild-type and mutant plants were prepared using

21

538 previously described pretreatment and hybridization methods (Lian et al., 2013). The
539 primers used to generate hybridization probes specific for *REV*, *PHB*, and *SPL/NZZ*
540 are listed in Supplemental Table S2. Digoxin (DIG)-labeled probes were prepared by
541 *in vitro* transcription (Roche, Mannheim, Germany) according to the manufacturer's
542 recommended protocol. Additionally, LNA (Locked Nucleic Acid) modified probes
543 specific for miR166 were synthesized and labeled with DIG at the 3'-end by TaKaRa
544 (Dalian, China).

545

546 **Reverse Transcription Quantitative PCR (RT-qPCR)**

547 Stage 3 anthers were carefully harvested from 6-week-old wild-type and mutant plants
548 under a stereo microscope and stored immediately in liquid nitrogen. Total RNA was
549 extracted from anthers with the RNeasy Plant Mini Kit (Qiagen, Hilden, Germany)
550 and then reverse-transcribed using oligo (dT) primers. Reverse transcription
551 quantitative PCR (RT-qPCR) analysis was completed with the Rotor-Gene 3000
552 system (Corbett Research, Mortlake, NSW, Australia) using SYBR Premix Ex Taq
553 (TaKaRa, Japan). *ACTIN* mRNA was used as an internal control, and relative mRNA
554 abundance was calculated as previously described (Liu et al. 2011). Primers specific
555 for *ACTIN*, *SPL/NZZ*, *REV*, *PHB*, *PHV*, *CNA*, and *ATHB8* (Supplemental Table S2)
556 were used to detect gene expression in the mutants.

557

558 **Chromatin immunoprecipitation assay**

559 The 35S: 3×Flag-mPHB transgenic plants were analyzed using a chromatin
560 immunoprecipitation (ChIP) assay. Inflorescence was crosslinked with 1% (v/v)
561 formaldehyde, and chromatin was isolated and precipitated as described (Zhang et al.,
562 2017). The crude chromatin extract was divided into three parts. One part was used as
563 the input control. The other two parts were used for immunoprecipitations with 5 µL
564 Flag antibodies (Sigma-Aldrich). After several washes, chromatin cross-linking was
565 reversed, and DNA was purified. qPCR (quantitative PCR) analysis was completed
566 using a MyiQ2 two-color real time PCR detection system, with immunoprecipitated
567 DNA as the template. Values for the ChIP samples were first normalized against that

22

568 of the input and then divided by the normalized Flag signal values to calculate the fold
569 enrichment. The sequences of the primers used to amplify different promoter regions
570 are listed in Supplemental Table S2.

571

572 **GR induction and RNA quantification**

573 The expression of the gene encoding the GR was induced as previously described
574 (Zhang et al., 2017). Seeds carrying the 35S:GR-mREV and 35S:GR-mPHB
575 constructs were plated on agar-solidified MS medium, and the resulting seedlings
576 were transplanted in soil. When the plants started to bolt, the inflorescences were
577 immersed in 0.1% (v/v) ethanol (mock), 10 μ M dexamethasone (DEX) in 0.1% (v/v)
578 ethanol, 10 μ M cycloheximide (CHX) in 0.1% (v/v) ethanol, or 10 μ M DEX and 10
579 μ M CHX in 0.1% (v/v) ethanol for 1 min. Post-treatment inflorescences were
580 harvested after 6 h of treatment. Total RNA was extracted using Trizol reagent
581 (Invitrogen) and then treated with RNase-free DNase (TaKaRa). RT-qPCR was
582 performed as described above using primers listed in Supplemental Table S2. The
583 experiment was repeated three times.

584

585 **YFP expression assay for protein-DNA interactions in tobacco leaves**

586 To measure the effects of PHB on the transcriptional regulation of *SPL/NZZ* and *WUS*,
587 the CDS of PHB was cloned into pCAMBIA1300 as an effector. The 2122-bp
588 sequences upstream of the *SPL/NZZ* coding regions and the 1650-bp sequence
589 upstream of the *WUS* coding regions were cloned into pCAMBIA3301 as reporters.
590 Type IIS restriction enzyme *Bsm*BI was used for construction of *SPL/NZZ* and *WUS*
591 promoters with binding sites mutation. *Agrobacterium* GV3101 strains carrying the
592 above verified constructs were introduced into *Nicotiana benthamiana* leaves. As
593 negative controls, leaves were infiltrated with strains carrying reporter with the
594 different *SPL/NZZ* and *WUS* promoters and empty effector. RNA was extracted from
595 the leaves of 3 days after infiltration and YFP expression were measured by RT-qPCR.

596

597 **Electrophoretic mobility shift assay**

23

598 The *PHB* and *REV* genes were cloned into the pMAL-c2x vector (New England
599 Biolabs, Ipswich, Massachusetts, USA) for the expression of a fusion protein with an
600 N-terminal MBP peptide. The prepared expression vectors as well as empty
601 pMAL-c2x vector (control) were inserted into competent *Escherichia coli* cells. The
602 fusion proteins were purified according to the manufacturer's recommended
603 procedure (E8021S). Additionally, DNA fragments from the SPL/NZZ promoter were
604 end-labeled with Cy5. The recombinant fusion protein (500 ng) in binding buffer (10
605 mM Tris-HCl, pH 7.6, 25 mM KCl, 2.5 mM MgCl₂, 1 mM EDTA, 1 mM DTT, and 10%
606 (v/v) glycerol) were supplemented with 10 ng Cy5-labeled DNA and incubated for 30
607 min at 25°C. The reaction mixtures were electrophoresed on 6% native
608 polyacrylamide gels in 0.5×TBE buffer (45mM Tris, 45mM boric acid, 1mM EDTA,
609 pH 8.0) at 200 V for 1.5 h. Gels were analyzed using a Tanon 4200SF
610 chemiluminescent imaging system (Shanghai, China).

611

612 **Statistical analysis**

613 The statistical analyses including Student's t-test were performed by Excel 2010
614 software. Both RT-qPCR and qPCR for each sample were replicated three times, the
615 average values of $2^{-\Delta CT}$ were used to determine the differences, and the data were
616 expressed as the mean \pm standard deviation (SD). A significant difference was
617 considered at $P < 0.05$, and extremely significant at $P < 0.01$.

618

619 **Accession numbers**

620 Sequence data from this article can be found in the Arabidopsis Genome Initiative or
621 GenBank/EMBL databases under the following accession numbers: *PHB*
622 (AT2G34710), *SPL/NZZ* (AT4G27330), *WUS* (AT2G17950), and *MIR166g*
623 (AT5G63715).

624

625 **Supplemental Data**

626 The following supplemental materials are available.

627

628 **Supplemental Figure S1.** Expression of miR166 and HD-ZIP III in the *jba-1D*

629 mutant with the abaxial side of the anther.

630 **Supplemental Figure S2.** The plant and flower of the *spl* mutant with the abaxial side
631 of the anther.

632 **Supplemental Figure S3.** Interaction between PHB and *SPL/NZZ*.

633 **Supplemental Figure S4.** The plant and flower of *spl-D* mutant.

634 **Supplemental Figure S5.** Expression levels of *SPL/NZZ* in the anthers of *jba-1D*,
635 *phb-7D*, and *spl-D* single and double mutants.

636

637 **Supplemental Table S1.** Mutants included in this study.

638 **Supplemental Table S2.** Probes and primers used in this study.

639

640 **Acknowledgements**

641 We thank Dr. N. Fedoroff (Pennsylvania State University, USA), Dr. J. Fletcher (Plant
642 Gene Expression Center, USA), Dr. Y. Helariutta (Department of Biosciences,
643 University of Helsinki, Finland), Dr. L.J. Qu (College of Life Sciences, Peking
644 University, China) and Dr. W.C. Yang (Institute of Genetics and Development,
645 Chinese Academy of Sciences, China) for providing mutant seeds. We thank Li Jiqin
646 (Shanghai Institute of Plant Physiology and Ecology, China) for helping us develop
647 the analyzed semi-sections.

648 This work was supported by grants from the National Key Research and
649 Development Program of China (Grant No.2016YFD0101900) and the Natural
650 Science Foundation of China (Grant Nos. 31771442 and 31571261).

651

652 **Competing interests**

653 The authors declare no competing financial interests.

654

655

656 **Table 1.** Microsporangium size in *phb-7D* and *jba-1D* mutants

Name	Parameters	IM	OM	FuM
C24	Length	329.3 ± 25.9	372.8 ± 30.3	-
	Width	87.3 ± 6.4	103.5 ± 10.2	-
<i>phb-7D</i>	Length	236.47 ± 43.9**	338.0 ± 43.4*	-
	Width	88.4 ± 11.1	100.7 ± 12.0	-
Col-7	Length	391.1 ± 51.0	410.0 ± 54.1	-
	Width	94.9 ± 11.9	105.0 ± 15.2	-
<i>jba-1D</i>	Length	-	-	373.4 ± 47.5*
	Width	-	-	161.5 ± 22.7**

IM, inner microsporangium; OM, outer microsporangium; FuM, fused microsporangium. Microsporangia of stage 12 anthers were measured, n ≥ 66 for each wild type and mutant. Each value is mean ± SD, * indicates statistical significance (t-test, * P < 0.05, ** P < 0.001).

657

658

659

660 **Figure Legends**

661

662 **Figure 1.** Formation of microsporangia and gene expression of HD-ZIP III genes and
 663 *SPL/NZZ* in the anthers of *phb-7D* and *jba-1D* mutants. (A) Scanning electron
 664 microscope (SEM) images showing the numbers and positions of microsporangia in
 665 anthers. Percentages of the anthers with the mutant phenotypes are shown. White
 666 asterisks indicate the remnants of shriveled microsporangia. Scale bars: 100 μm.
 667 scanning electron micrographs of *phb-7D* were digitally abstracted and made into a
 668 composite for comparison. (B) RT-qPCR showing relative expression of HD-ZIP III
 669 genes in the *jba-1D* and *phb-7D* anthers (mild category) at stage 3. (C) Cross sections
 670 of anthers of the wild-type, *jba-1D*, and *phb-7D* mutants. eBD, ectopic boundary
 671 tissue; eMsc, ectopic microsporocyte; FuM, fused microsporangium; Msc,
 672 microsporocytes; Msp, microspores; OM, outer microsporangium; PG, pollen grains;
 673 PP, primary parietal cells; PS, primary sporogenous cells; rIM, remnants of inner
 674 microsporangia; StR, stomium region. Asterisks indicate the remnants of undeveloped
 675 microsporangia. Scale bars: 20 μm. (D) The ratio of number of microsporocytes per
 676 locule in the mutants to the wild type. More than 30 locules for the *phb-7D* mutant
 677 with mild phenotype or the *jba-1D* mutant were observed. (E) RT-qPCR showing
 678 relative expression of *SPL/NZZ* gene in the *jba-1D* and *phb-7D* anthers at stage 3.
 679 Three biological replicates were analyzed in (B) and (E). Error bars indicate the
 680 standard deviation while black asterisks show significant difference at the 0.05 and
 681 0.01 levels in *t*-test. IM, inner microsporangium; OM, outer microsporangium; FuM,
 682 fused microsporangium.

683

684 **Figure 2.** Expression domains of miR165/6, miR165/6-targeted genes, and *SPL/NZZ*

26

685 in anthers. (A) RNA *in situ* hybridization showing the expression domains of miR166,
686 *REV*, *PHB*,*k* and *SPL/NZZ*. (B) Schematic diagrams indicating the rearranged
687 expression domains of *PHB* and *SPL/NZZ* during anther development. Ca, carpel;
688 Msc, microsporocytes; PP, primary parietal cells; PS, primary sporogenous cells; V,
689 vasculature. White arrowheads show the stomium regions. Asterisks indicate the
690 remnants of shriveled microsporangia. Scale bars: 20 μ m.

691

692 **Figure 3.** Anther morphology and anatomy in the single and double mutants of
693 *SPL/NZZ*, *MIR166g*, and *PHB*. (A) Anthers of *spl*, *jba-1D*, and *phb-7D* mutants at
694 stage 12. (B) SEM images showing the appearance of *spl*, *jba-1D*, and *phb-7D* anthers
695 at stage 12. (C) Whole-mount clearing images showing the internal structures of *spl*,
696 *jba-1D*, and *phb-7D* locules at stage 12. (D) Magnified images of (c) showing the
697 pollen grains in *spl*, *jba-1D*, and *phb-7D* locules at stage 12. (E) Cross sections of *spl*,
698 *jba-1D*, and *phb-7D* anthers. (F) Plant phenotypes of *phb-7D*, *spl-D/+*, and *jba-1D*
699 single and double mutants at flowering stage. (G) The distribution of *phb-7D spl-D/+*
700 anthers with the mutant phenotypes of different severity. (H) Anthers of *phb-7D*,
701 *spl-D/+*, and *jba-1D* single and double mutants at stage 11 under anatomical
702 microscope. (I) SEM images showing the appearance of anthers of the *phb-7D*,
703 *spl-D/+*, and *jba-1D* single and double mutants at stage 11. (J) Cross sections of the
704 anthers of *phb-7D*, *spl-D/+*, and *jba-1D* single and double mutants at stage 11.
705 Arrowheads indicate the dehiscence zones in *phb-7D jba-1D* anther. Asterisks
706 indicate the thin boundary between inner and outer microsporangia. Scale bars: 50 μ m
707 (A-C, H, J); 20 μ m (E, J).

708

709 **Figure 4.** Binding of PHB in the promoter of *SPL/NZZ*. (A) Diagram of *SPL/NZZ*
710 genomic regions showing the positions of putative binding sites (S1-S6). The gray and
711 black boxes indicate the UTR and exon regions, respectively, while the lines indicate
712 intergenic regions and introns. Arrow heads above the lines indicate the putative
713 binding sites. (B) Electrophoretic mobility shift assay (EMSA) showing the binding
714 affinity of the putative sites of *SPL/NZZ* promoter regions by PHB. The positions of
715 PHB-DNA complexes are marked by shifted bands. (C) Competitor DNA binding
716 assay showing the binding affinity of S4 site of the *SPL/NZZ* promoter regions by
717 PHB. (D) Sequences of S4 site and its competitor DNA. (E) ChIP assays showing
718 PHB binding to the *SPL/NZZ* promoter. (F) DNA sequences of the wild-type *SPL/NZZ*
719 promoter and mutant *SPL/NZZ* promoters. (G) Structure of the *SPL/NZZ*
720 promoter-driven *YFP* reporter gene. The *SPL/NZZ* promoter, 35S promoter, *YFP*, *GUS*,
721 and *PHB* genes are indicated. (H) Relative reporter (*YFP*) expression in plants with
722 different *SPL/NZZ* promoters. *Nicotiana benthamiana* leaves were transfected with the
723 reporter (*pSPL/NZZ*, *pSPL/NZZm1*, *pSPL/NZZm2*) and the effectors (mPHB). (I)
724 RT-qPCR showing relative expression of *SPL/NZZ* in *p35S::GR-mPHB* lines treated
725 with DEX and DEX+CHX solutions. Three biological replicates were analyzed. Error
726 bars indicate the standard deviation while asterisks show significant difference at the
727 0.05 and 0.01 levels in *t*-test.

728

729 **Figure 5.** Binding of PHB in the promoter of *WUS*. (A) In situ hybridization showing
730 the expression patterns of *WUS* in developing anthers of *jba-1D* and *phb-7D* mutants.
731 StR, stomium regions. Scale bars: 50 μ m (B) Putative binding sites of PHB in *WUS*. *a*,
732 *b*, *c*, *d*, *e*, *f*, and *g* represent seven putative binding sites in *WUS*. The yellow mark
733 indicates a 57-bp regulatory region (-655bp ~ -712bp) conferring *WUS* transcription in
734 the SAM stem cell niche (C) EMSA showing the binding affinity of the putative sites
735 of *WUS* promoter regions by PHB. The positions of PHB-DNA complexes are marked
736 by shifted band. (D) ChIP assays showing PHB binding to the *WUS* promoter. (E)
737 RT-qPCR showing relative expression of *WUS* in *phb-7D* and *jba-1D*. (F) DNA
738 sequences of the wild-type *WUS* promoter and mutant *WUS* promoters with mutations
739 in different binding sites. (G) Schematic diagram of the reporter (*pWUS*, *pWUSm1*,
740 *pWUSm2*) and effector (*mPHB*) constructs. (H) RT-qPCR showing relative expression
741 of YFP measured after transient transformation of the reporter (*pWUS*, *pWUSm1*,
742 *pWUSm2*) and effector (*mPHB*) constructs in *Nicotiana benthamiana* leaves. (I)
743 RT-qPCR showing relative expression of *WUS* in *p35S::GR-mPHB* lines treated with
744 DEX and DEX+CHX solutions. Three biological replicates were analyzed. Error bars
745 indicate the standard deviation while asterisks show significant difference at the 0.05
746 and 0.01 levels in *t*-test.

747

748 **Figure 6.** Model for miR165/6 regulation of *SPL/NZZ* in formation of the boundary
749 between inner and outer microsporangia in anthers. During anther development,
750 miR165/6 silence *PHB* by complementary sequences. PHB binds to *SPL/NZZ* to
751 inhibit the activity of *SPL/NZZ*. miR165/6 and *SPL/NZZ* domains move from the
752 two lateral regions of stamens to the four corners of anthers and then to
753 microsporangia while *PHB* domains are migrated from the middle regions of thecae to
754 the boundary between inner and outer microsporangia and then to the stomium
755 regions. PHB facilitates the formation of the boundary where it determines the
756 formation of stomium through *WUS* but inhibits the differentiation of microsporocytes.
757 *SPL/NZZ* promotes the initiation of microsporocytes but obstructs the formation of
758 the boundary. BD, boundary between inner and outer microsporangia; IM, inner
759 microsporangia; OM, outer microsporangia; SR, stomium region.

760

761

762

Parsed Citations

- Bäurle I1, Laux T (2005) Regulation of WUSCHEL transcription in the stem cell niche of the Arabidopsis shoot meristem. Plant Cell 17: 2271-2280**
Pubmed: [Author and Title](#)
Google Scholar: [Author Only](#) [Title Only](#) [Author and Title](#)
- Bowman JL (2004) Class III HD-Zip gene regulation, the golden fleece of ARGONAUTE activity? BioEssays 26: 938-942**
Pubmed: [Author and Title](#)
Google Scholar: [Author Only](#) [Title Only](#) [Author and Title](#)
- Brandt R, Salla-Martret M, Bou-Torrent J, Musielak T, Stahl M, Lanz C, Ott F, Schmid M, Greb T, Schwarz M, Choi SB, Barton MK, Reinhart BJ, Liu T, Quint M, Palauqui JC, Martinez-García JF, Wenkel S (2012) Genome-wide binding-site analysis of REVOLUTA reveals a link between leaf patterning and light-mediated growth responses. Plant J 72: 31-42**
Pubmed: [Author and Title](#)
Google Scholar: [Author Only](#) [Title Only](#) [Author and Title](#)
- Carlsbecker A, Lee JY, Roberts CJ, Dettmer J, Lehesranta S, Zhou J, Lindgren O, Moreno-Risueno MA, Vate ´n A, Thitamadee S, Campilho A, Sebastian J, Bowman JL, Helariutta Y, Benfey PN (2010) Cell signalling by microRNA165/6 directs gene dose-dependent root cell fate. Nature 465: 316-321**
Pubmed: [Author and Title](#)
Google Scholar: [Author Only](#) [Title Only](#) [Author and Title](#)
- Dinneny JR, Weigel D, Yanofsky M (2006) NUBBIN and JAGGED define stamen and carpel shape in Arabidopsis. Development 133: 1645-1655**
Pubmed: [Author and Title](#)
Google Scholar: [Author Only](#) [Title Only](#) [Author and Title](#)
- Deyhle F1, Sarkar AK, Tucker EJ, Laux T (2007) WUSCHEL regulates cell differentiation during anther development. Dev Biol 302: 154-159**
Pubmed: [Author and Title](#)
Google Scholar: [Author Only](#) [Title Only](#) [Author and Title](#)
- Emery JF, Floyd SK, Alvarez J, Eshed Y, Hawker NP, Izhaki A, Baum SF, Bowman JL (2003) Radial patterning of Arabidopsis shoots by class III HD-ZIP and KANADI genes. Curr. Biol 13: 1768-1774**
Pubmed: [Author and Title](#)
Google Scholar: [Author Only](#) [Title Only](#) [Author and Title](#)
- Eshed Y, Baum SF, Perea JV, Bowman JL (2001) Establishment of polarity in lateral organs of plants. Curr. Biol 11: 1251-1260**
Pubmed: [Author and Title](#)
Google Scholar: [Author Only](#) [Title Only](#) [Author and Title](#)
- Feng X, Dickinson HG (2007) Packaging the male germline in plants. Trends Genet 23: 503-510**
Pubmed: [Author and Title](#)
Google Scholar: [Author Only](#) [Title Only](#) [Author and Title](#)
- Feng X, Dickinson HG (2009) Cell-Cell communication in plant reproduction. Biochem Soc Trans 38: 571-576**
Pubmed: [Author and Title](#)
Google Scholar: [Author Only](#) [Title Only](#) [Author and Title](#)
- Goldberg R, Beals T, Sanders P (1993) Anther development: basic principles and practical applications. Plant Cell 5: 1217-1229**
Pubmed: [Author and Title](#)
Google Scholar: [Author Only](#) [Title Only](#) [Author and Title](#)
- Hord CL, Chen C, Deyoung BJ, Clark SE, Ma H (2006) The BAM1/BAM2 receptor-like kinases are important regulators of Arabidopsis early anther development. Plant Cell 18: 1667-1680**
Pubmed: [Author and Title](#)
Google Scholar: [Author Only](#) [Title Only](#) [Author and Title](#)
- Ito T, Wellmer F, Yu H, Das P, Ito N, Alves-Ferreira M, Riechmann JL, Meyerowitz EM (2004) The homeotic protein AGAMOUS controls microsporogenesis by regulation of SPOROCTELESS. Nature 430: 356-360**
Pubmed: [Author and Title](#)
Google Scholar: [Author Only](#) [Title Only](#) [Author and Title](#)
- Li LC, Qin GJ, Tsuge T, Hou XH, Ding MY, Aoyama A, Oka T, Chen ZL, Gu H, Zhao YD, Qu LJ (2008) SPOROCTELESS modulates YUCCA expression to regulate the development of lateral organs in Arabidopsis. New Phytol 179: 751-764**
Pubmed: [Author and Title](#)
Google Scholar: [Author Only](#) [Title Only](#) [Author and Title](#)
- Lian H, Li X, Liu Z, He Y (2013) HYL1 is required for establishment of stamen architecture with four microsporangia in Arabidopsis. J Exp Bot 64: 3397-3410**
Pubmed: [Author and Title](#)
Google Scholar: [Author Only](#) [Title Only](#) [Author and Title](#)

Liu ZY, Jia LG, Wang H, He YK (2011) HYL1 regulates the balance between adaxial and abaxial identity for leaf flattening via miRNA-mediated pathways. *J Exp Bot* 62: 4367-4381

Pubmed: [Author and Title](#)

Google Scholar: [Author Only](#) [Title Only](#) [Author and Title](#)

Ma H (2005) Molecular genetic analyses of microsporogenesis and microgametogenesis in flowering plants. *Annu Rev Plant Biol* 56: 393-434

Pubmed: [Author and Title](#)

Google Scholar: [Author Only](#) [Title Only](#) [Author and Title](#)

McConnell JR, Emery J, Eshed Y, Bao N, Bowman JH, Barton MK (2001) Role of PHABULOSA and PHAVOLUTA in determining radial patterning in shoots. *Nature* 411: 709-713

Pubmed: [Author and Title](#)

Google Scholar: [Author Only](#) [Title Only](#) [Author and Title](#)

Sanders PM, Bui AQ, Weterings K, McIntire KN, Hsu YC, Lee PY, Truong MT, Beals TP, Robert B, Goldberg RB (1999) Anther developmental defects in *Arabidopsis thaliana* male-sterile mutants. *Sex Plant Rep* 11: 297-322

Pubmed: [Author and Title](#)

Google Scholar: [Author Only](#) [Title Only](#) [Author and Title](#)

Schiefthaler U, Balasubramanian S, Sieber P, Chevalier D, Wisman E, Schneitz K (1999) Molecular analysis of NOZZLE, a gene involved in pattern formation and early sporogenesis during sex organ development in *Arabidopsis thaliana*. *Proc Natl Acad Sci USA* 96: 11664-11669

Pubmed: [Author and Title](#)

Google Scholar: [Author Only](#) [Title Only](#) [Author and Title](#)

Scott RJ, Spielman M, Dickinson HG (2004) Stamen structure and function. *Plant Cell* 16: S46-S60

Pubmed: [Author and Title](#)

Google Scholar: [Author Only](#) [Title Only](#) [Author and Title](#)

Smith Z Long J (2010) Control of *Arabidopsis* apical-basal embryo polarity by antagonistic transcription factors. *Nature* 464: 423-426

Pubmed: [Author and Title](#)

Google Scholar: [Author Only](#) [Title Only](#) [Author and Title](#)

Smyth DR, Bowman JH, Meyerowitz EM (1990) Early flower development in *Arabidopsis*. *Plant Cell* 2: 755-767

Pubmed: [Author and Title](#)

Google Scholar: [Author Only](#) [Title Only](#) [Author and Title](#)

Toriba T, Suzaki T, Yamaguchi T, Ohmori Y, Tsukaya H, Hirano H (2010) Distinct regulation of adaxial-abaxial polarity in anther patterning in rice. *Plant Cell* 22: 1452-1462

Pubmed: [Author and Title](#)

Google Scholar: [Author Only](#) [Title Only](#) [Author and Title](#)

Williams L, Grigg S, Xie M, Christensen S, Fletcher J (2005) Regulation of *Arabidopsis* shoot apical meristem and lateral organ formation by microRNA miR166g and its AtHD-ZIP target genes. *Development* 132: 3657-3668

Pubmed: [Author and Title](#)

Google Scholar: [Author Only](#) [Title Only](#) [Author and Title](#)

Wu F, Yu L, Cao W, Mao Y, Liu Z, He Y (2007) The N-terminal double-stranded RNA binding domains of *Arabidopsis* HYPONASTIC LEAVES1 are sufficient for pre-microRNA processing. *Plant Cell* 19: 914-925

Pubmed: [Author and Title](#)

Google Scholar: [Author Only](#) [Title Only](#) [Author and Title](#)

Yang W, Ye D, Xu J, Sundaresan V (1999) The SPOROCTELESS gene of *Arabidopsis* is required for initiation of sporogenesis and encodes a novel nuclear protein. *Genes Dev* 13: 2108-2117

Pubmed: [Author and Title](#)

Google Scholar: [Author Only](#) [Title Only](#) [Author and Title](#)

Yang X, Ren W, Zhao Q, Zhang P, Wu F, He Y (2014) Homodimerization of HYL1 ensures the correct selection of cleavage sites in primary miRNA. *Nucleic Acids Res* 42: 12224-12236

Pubmed: [Author and Title](#)

Google Scholar: [Author Only](#) [Title Only](#) [Author and Title](#)

Yuan L, Sundaresan V (2015) Spore formation in plants: sporocyteless and more. *Cell Res* 25: 7-8

Pubmed: [Author and Title](#)

Google Scholar: [Author Only](#) [Title Only](#) [Author and Title](#)

Zhang TQ, Lian H, Zhou CM, Xu L, Jiao Y, Wang JW (2017) A two-step model for de novo activation of WUSCHEL during plant shoot regeneration. *Plant Cell* 29: 1073-1087

Pubmed: [Author and Title](#)

Google Scholar: [Author Only](#) [Title Only](#) [Author and Title](#)

Zhao D (2009) Control of anther cell differentiation: a teamwork of receptor-like kinases. *Sex Plant Reprod* 22: 221-228

Pubmed: [Author and Title](#)

Google Scholar: [Author Only](#) [Title Only](#) [Author and Title](#)

Zhong R, Ye Z (1999) IFL1, a gene regulating interfascicular fiber differentiation in Arabidopsis, encodes a Homeodomain–Leucine Zipper protein. Plant Cell 11: 2139-2152

Pubmed: [Author and Title](#)

Google Scholar: [Author Only](#) [Title Only](#) [Author and Title](#)

Zhong R, Ye Z (2004) amphivasal vascular bundle 1, a gain of-function mutation of the IFL1/REV gene, is associated with alterations in the polarity of leaves, stems and carpels. Plant Cell Physiol 45: 369–385

Pubmed: [Author and Title](#)

Google Scholar: [Author Only](#) [Title Only](#) [Author and Title](#)